ELSEVIER

Contents lists available at ScienceDirect

Manufacturing Letters

journal homepage: www.elsevier.com/locate/mfglet



Letters

Design and fabrication of pH-responsive monodisperse gold/peptide/gold sandwich nanoparticles



Wei Li^a, Zimeng Zhang^a, Yuchen Liu^a, Jingjing Qiu^{c,*}, Shiren Wang^{a,b,*}

- ^a Department of Industrial and Systems Engineering, Texas A&M University, College Station, TX 77843, United States
- ^bDepartment of Materials Science and Engineering, Texas A&M University, College Station, TX 77843, United States
- ^c Department of Mechanical Engineering, Texas A&M University, College Station, TX 77843, United States

ARTICLE INFO

Article history: Received 16 September 2022 Received in revised form 22 January 2023 Accepted 23 March 2023 Available online 7 April 2023

Keywords: Sandwich nanostructures Nanofabrication Nanoparticles pH-responsive Peptide

ABSTRACT

Integrating stimuli-responsive molecules and plasmonic nanoparticles into a single nanoscale platform for stimuli-adaptive functionality is of great importance in nanotechnology. However, existing strategies for constructing stimuli-responsive molecule/noble metal composite nanoparticles based on a solution or solid-phase methods result in limited separation efficiency and low structural precision. Here, we propose a solid-solution combined strategy to prepare monodisperse pH-adaptive gold/peptide/gold sandwich nanoparticles with precisely controlled layered structures. Wafer-scale gold/peptide/gold layered structure was first deposited on a silicon wafer and then etched by argon plasma using silica nanoparticles as a mask. Sandwich nanoparticles can be easily released from silicon wafers by a wet etching reaction and then purified by centrifugation. The as-prepared gold/peptide/gold nanoparticles exhibit distinct localized surface plasmon resonance (LSPR) coupling peaks at near-infrared wavelengths in acidic and neutral environments, demonstrating their great potential as pH-responsive optical nanodevices. In addition, this flexible and configurable approach enables the precise fabrication of layered nanostructures of different sizes, layer numbers, and compositions, with wide applications in optical actuation and sensors.

© 2023 Society of Manufacturing Engineers (SME). Published by Elsevier Ltd. All rights reserved.

1. Introduction

Integrating different functional components into a single nanoscale platform to realize multiple purposes is of great importance in various emerging applications [1-4]. Gold nanoparticles (AuNPs) have emerged as promising optical actuation and sensing materials due to their excellent physicochemical properties, good biocompatibility, and tunable localized surface plasmon resonance (LSPR) characteristics [5,6]. To adaptively tune the LSPR coupling of adjacent AuNPs in different environments, a monodisperse stimulusresponsive AuNP/polymer/AuNP sandwich nanostructure is highly desired. Many existing research works can statically and precisely manipulate the gap between AuNPs through short molecules such as DNA or RNA. For example, Lim et al. reported highly uniform and reproducible surface-enhanced Raman scattering from DNAtailorable AuNPs with a 1-nm interior gap [7]. Smith et al. have assembled DNA-functionalized AuNPs with gaps and overhangs in linker DNA [8]. However, these works can only control the gap statically, and dynamic manipulation of the gap between AuNPs is highly desired. Carboxy- and amine-containing peptides [9,10]

E-mail addresses: Jennyqiu@tamu.edu (J. Qiu), s.wang@tamu.edu (S. Wang).

are widely used to achieve pH-responsivity in biomedical research. However, integrating ultrathin pH-responsive molecular layers (less than 5 nm thick) between two gold nanodiscs with designed interparticle gaps is challenging.

Preparation of plasmonic metal/polymer/metal sandwich nanocomposites using a solution-based bottom-up approach yields a mixture of dimers, trimers, and other large nanoclusters [11]. In addition, the gap between plasmonic NPs in a single composite nanostructure cannot be precisely controlled, resulting in broad spectral absorption peaks [12]. Solid-phase top-down synthesis techniques such as hole-mask nanolithography [13] and E-beam lithography [14] can synthesize NPs by trimming rationally designed solid substrates. For example, Juluri et al. fabricated shape-uniform gold nanodiscs by Ar plasma etching of gold film, with polystyrene nanoparticles as masks [15]. Compared with solution-based strategies, solid-phase lithography can precisely control layered structures. However, solid-phase methods have not been applied to fabricate monodisperse metal/molecule/metal sandwich NPs, which need to be uniform in size, not easily disintegrated, and dispersible in aqueous solutions.

In this study, we demonstrate a novel strategy combining directional physical ion etching and isotropic wet chemical etching to fabricate gold/peptide/gold sandwich NPs with different structures

^{*} Corresponding authors.

and sizes, see Fig. 1. The morphology of the gold/peptide/gold sandwich NPs in each synthesis step was characterized by scanning electron microscopy (SEM) and transmission electron microscopy (TEM). The dispersibility and pH-responsive spectral absorption in aqueous solution were confirmed by dynamic light scattering (DLS) and UV-Vis-NIR absorption spectroscopy, respectively.

2. Materials and methods

2.1. Materials

Silicon wafers (EPI coating) were purchased from Addison Engineering. Gold pellets and chromium pellets evaporation materials were purchased from Kurt J. Lesker Company. Peptides with amino acids sequence Cys-Pro-Glu-Glu-Glu-Cys (Mw = 708) were provided by Biomatik. Monodisperse suspensions of aminated silica nanospheres (10 mg/ml, in ethanol) with different diameters (60, 120, and 300 nm) were purchased from nanoComposix. Gold etchant, chromium etchant, thiol terminated PEG (Mw = 3000), trisodium citrate dihydrate, and 4-Aminothiophenol (4-ATP) were purchased from Sigma-Aldrich.

2.2. Synthesis of gold/peptide/gold structure on silicon wafers

Synthesis steps for gold/peptide/gold structure on a silicon wafer are illustrated in Fig. 1a and Fig. 2a. First, Cr film (5 nm thick)

and gold film (15–30 nm thick) were deposited on the piranhatreated silicon wafers (13 mm \times 13 mm) [16] by thermal evaporation (Oxford Vacuum Science, 10^{-5} mbar). The deposition rate was around 0.1 nm/s. Subsequently, the gold-coated wafers were immersed in an aqueous sodium citrate solution (1 mM) for 3 h to negatively charge the gold surface. The wafers were then immersed in a 3 mM peptide aqueous solution for 24 h, allowing the peptide to self-assemble on the gold surface and to form a dense peptide brush layer via thiol chemistry. Afterward, the peptide-coated wafers were immersed in water for 1 h to remove physically absorbed citrate and peptides. After drying, a second gold layer (15–30 nm thick) was deposited on the peptide-coated wafer by thermal evaporation.

2.3. Tailoring of gold/peptide/gold sandwich NPs by lithography

The steps for tailoring gold/peptide/gold sandwich NPs by lithography are illustrated in Fig. 1a to 1c. The gold/peptide/gold coated wafers were immersed in 4-ATP aqueous solution (3 mM) for 10 min to enhance the hydrophilicity of the gold surface. Then, a monolayer of silica NPs was spin-coated (WS-400-6NPP Spin Coater) on top of the gold layer at 2500 rpm. In spin-coating, the concentrations of 60 nm, 120 nm, and 300 nm silica NPs were set at 1 wt%, 1.5 wt%, and 2 wt%, respectively. CHF₃ RIE (Oxford Plasmalab 100 Plus, 0.5–3 min) can be applied to adjust the size of silica NPs. The samples were then etched for 2–6 min using physical ion etching (argon gas) [17]. The redeposited gold on the surface of

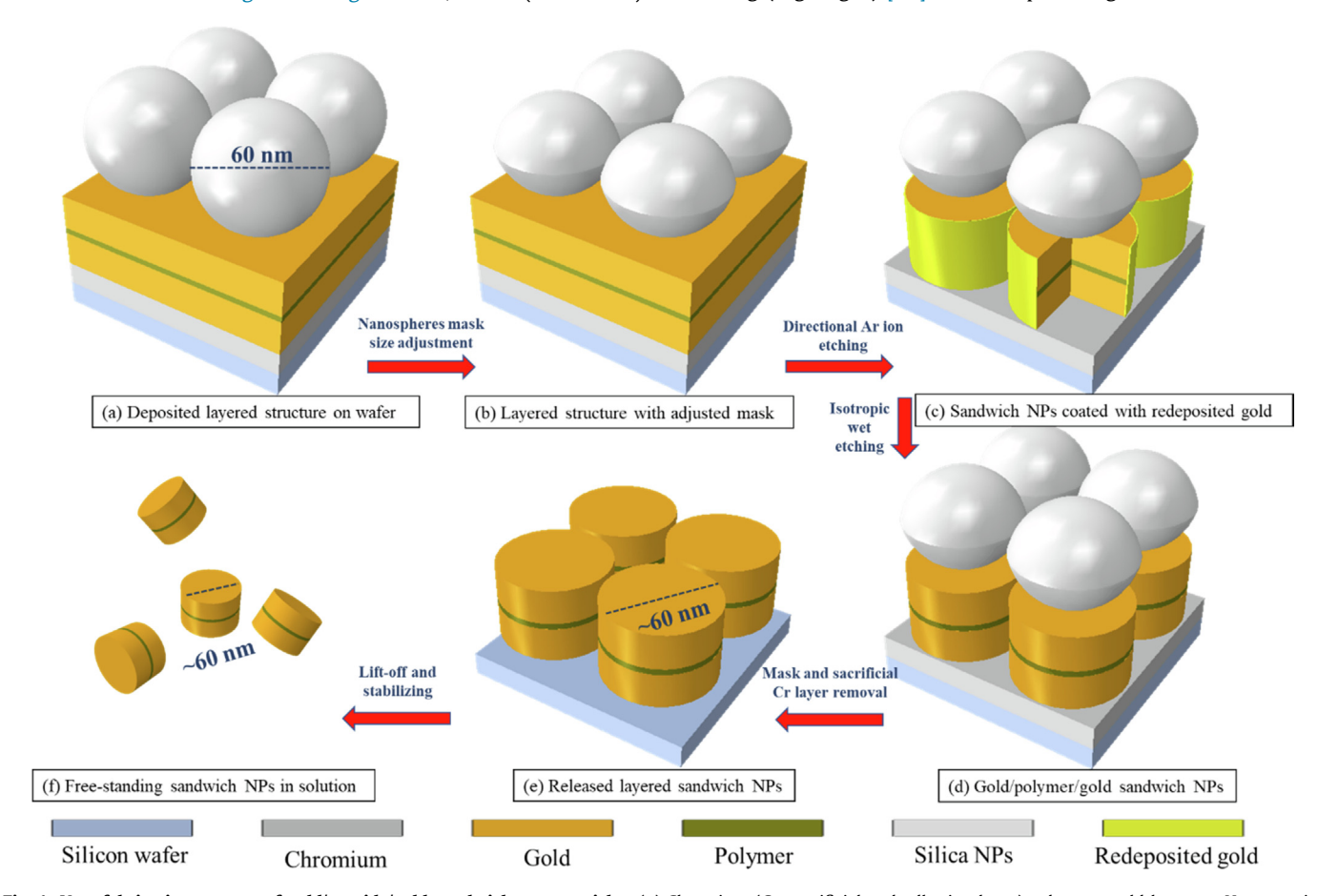


Fig. 1. Nanofabrication process of gold/peptide/gold sandwich nanoparticles. (a) Chromium (Cr, sacrificial and adhesion layer), a bottom gold layer, a pH-responsive peptide layer, a top gold layer, and silicon NPs (60 nm diameter shown here) are sequentially deposited on clean silicon wafers via thermal vapor disposition, self-assembly, or spin-coating techniques. (b) RIE (CHF₃) is used to adjust the size of the silica NPs mask for further etching. (c) With silica NPs masks, the plasmonic sandwich nanostructure can be obtained by directional Ar ion etching. (d) The redeposited gold debris on the substrate can be removed by wet etching using dilute gold etchant (1 wt% KI/I₂ solution). (e) The residual silica NPs masks can be removed by bath sonication in water. (f) The sacrificial Cr layer can be effectively removed by wet etching, and then the monodisperse sandwich NPs can be released from the substrate.

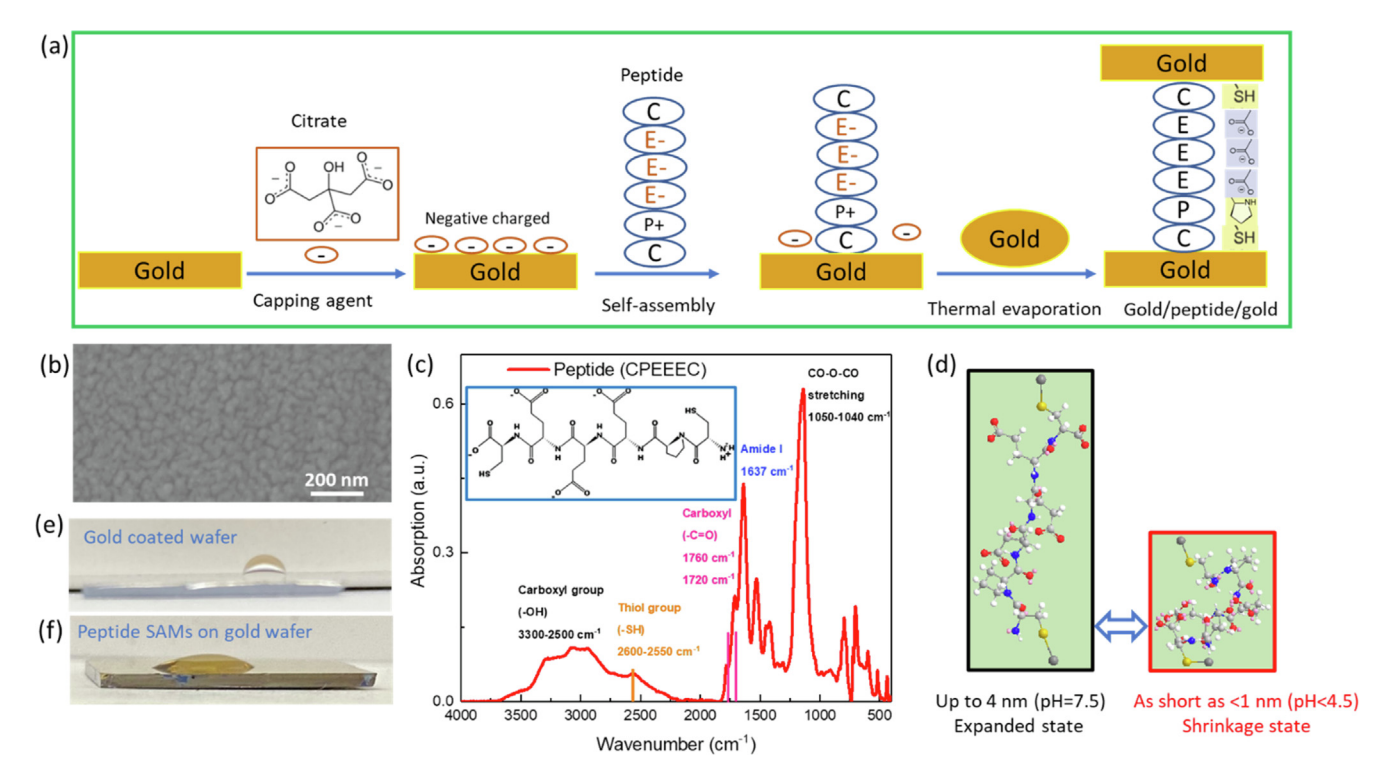


Fig. 2. Design and fabrication of wafer-scale gold/peptide/gold sandwich structures. (a) Schematic diagram of the fabrication steps of the gold/peptide/gold layered structure on a wafer. (b) Thermally evaporated gold on a silicon wafer. (c) FTIR spectra of the pH-responsive peptide (CPEEC amino acids). (d) Schematic of the pH-responsive peptide in the expanded and shrinkage states. (e-f) Water contact angles on the gold surface before and after peptide self-assembly.

gold/peptide/gold sandwich NPs was then removed using a dilute gold etchant (KI/I_2 iodine-iodide system, 1 wt%) for 3 s.

2.4. Release, PEGylation, and purification of gold/peptide/gold sandwich NPs

The steps to release, PEGylate, and purify the gold/peptide/gold sandwich NPs are illustrated in Fig. 1d to 1e. The silicon wafers were bath sonicated in DI water for 2 min to remove residual silica NPs masks and then immersed in dilute aqueous PEG-SH solution (1 mM) for 24 h to partially PEGylate the NPs. Afterward, the wafers were immersed in Cr etchant (1 wt%) to dissolve the sacrificial Cr layer and release the partially PEGylated NPs into the solution. The resulting solution was centrifuged (Eppendorf Centrifuge 5810R) at 200 rpm to remove the impurity-containing pellet. The supernatant was then centrifugated at 12000 rpm to remove the dissolved ions. The resulting pellet was dispersed in dilute aqueous PEG-SH solution (1 mM) by bath sonication and kept for 24 h to fully PEGylate the NPs. After centrifugation at 12000 rpm to remove the excess PEG-SH in the solution, the pellet was then dispersed in DI water to obtain well-dispersed PEGylated gold/peptide/gold sandwich NPs.

2.5. Characterizations and simulation

The morphology of the as-prepared NPs was characterized by field emission scanning electron microscopy (JEOL JSM-7500F) and transmission electron microscopy (JEOL 2020, operated at 200 kV). Fourier transform infrared (FTIR) spectra were obtained with a Bruker ALPHA-Platinum using the ATR (Attenuated Total Reflection) method. Dynamic Light Scattering (DLS) was characterized by Zetasizer Nano ZS. The UV-Vis-NIR absorption spectra were measured by Hitachi U-4100. Electrodynamic calculations were

performed with COMSOL Multiphysics using the Finite-Difference Time-Domain (FDTD) method [18].

3. Results and discussion

3.1. Design and fabrication of wafer-scale gold/peptide/gold sandwich structures

To fabricate gold/peptide/gold sandwich NPs, a wafer-scale gold/peptide/gold structure was first deposited on a wafer, see Fig. 2a. The gold film prepared on the silicon wafer by thermal evaporation demonstrates a polycrystalline structure with a flat surface, see Fig. 2b. The structure of peptides can be designed to achieve different stimulus responses (such as pH, temperature, and metal ions) based on the sequence of amino acids [10]. To ensure the connection between the peptide and gold, the terminal amino acids of the peptide should be cysteine, and its thiol group can form an Au-S bond with gold. To achieve pH response, a peptide consisting of 6 amino acids (Cys-Pro-Glu-Glu-Glu-Cys) was synthesized, see Fig. 2c. Among the amino acids, the three glutamic acids contain three pH-responsive carboxy groups, see Fig. 2d. When the pH is above 5, the carboxy group is deprotonated and negatively charged, and the peptide is in an extended state (up to 4 nm in length). At pH values below 4.5, the carboxy group is protonated and electrically neutral, and the peptide is in a shrinkage state (can be less than 1 nm in length). After the peptides selfassembled on the gold surface, the water contact angle of the gold film decreased from 78.4° to 32.4°, see Fig. 2e and 2f. The increased hydrophilicity indicates the formation of a dense peptide film on the gold surface. After the thermal evaporation of another gold layer, a wafer-scale gold/peptide/gold sandwich structure was obtained on the wafer. The gold/peptide/gold coated wafers were put on a hot plate (~80 °C) for 1 h to facilitate the Au-S bonding between the top gold layer and peptide by enhancing the activity of the thiol groups.

3.2. Preparation of monodisperse gold/peptide/gold sandwich nanoparticles

As shown in Fig. 3a, silica NPs (300 nm) were spin-coated in a monolayer on gold/polymer/gold-coated wafers. The size of the silica NPs mask can be further reduced by CHF₂ RIE, see Fig. 3b. Typically, thin gold films are patterned by wet etching or chlorine-based reactive ion etching (RIE), but these isotopic chemical etching methods cause severe mask undercuts [17,19] and lead to nanoscale feature loss. To minimize the undercutting, physical ion etching (argon) was used to etch gold in this study, which etched the gold directionally and produced well-defined sandwich NPs with straight sidewalls, see Fig. 3c. However, the low volatility of gold resulted in massive etched gold debris redepositing on the sandwich NPs and sealing the peptide layer (Fig. 3d), preventing the pH-responsive peptides from interacting with surrounding solution. To this problem, this study innovatively used a diluted gold etchant (1 wt% KI/I₂) to wet-etch redeposited gold on the surface of gold/peptide/gold sandwich NPs, thereby exposing the peptide layer. After removing the residual silica mask by bath sonication, well-shaped gold/peptide/gold sandwich NPs were obtained on the silicon wafer, see Fig. 3e. These gold/peptide/gold sandwich NPs were released from the wafers after wet etching away the Cr sacrificial layer. As shown in Fig. 3f, after PEGylation and purification, monodisperse gold/peptide/gold NPs were obtained in an aqueous solution, which can be used as pH-responsive optical nanodevices.

3.3. Preparation of sandwich nanoparticles with different sizes

This flexible and configurable approach enables the preparation of various layered nanostructures with different sizes and compositions. As shown in Fig. 3g to 3i, gold/peptide/gold sandwich NPs with a diameter of 120 nm were prepared using 120 nm silica NPs as masks. As shown in Fig. 4a and 4b, pH-responsive gold/peptide/gold sandwich NPs with a diameter of 60 nm were prepared using 60 nm silica NPs as masks. The hydrodynamic diameter of the 60 nm gold/peptide/gold sandwich NPs is about 69 nm, which is in good agreement with the designed sandwich dimensions (two 15 nm thick gold nanodiscs, one 4 nm thick peptide film), see Fig. 4c. The hydrodynamic diameter of the single-layer gold nanodisc is about 21 nm, which also fits well with the designed dimension (15 nm thick, 60 nm diameter). These results indicate that the method for preparing sandwich NPs proposed in this study is efficient.

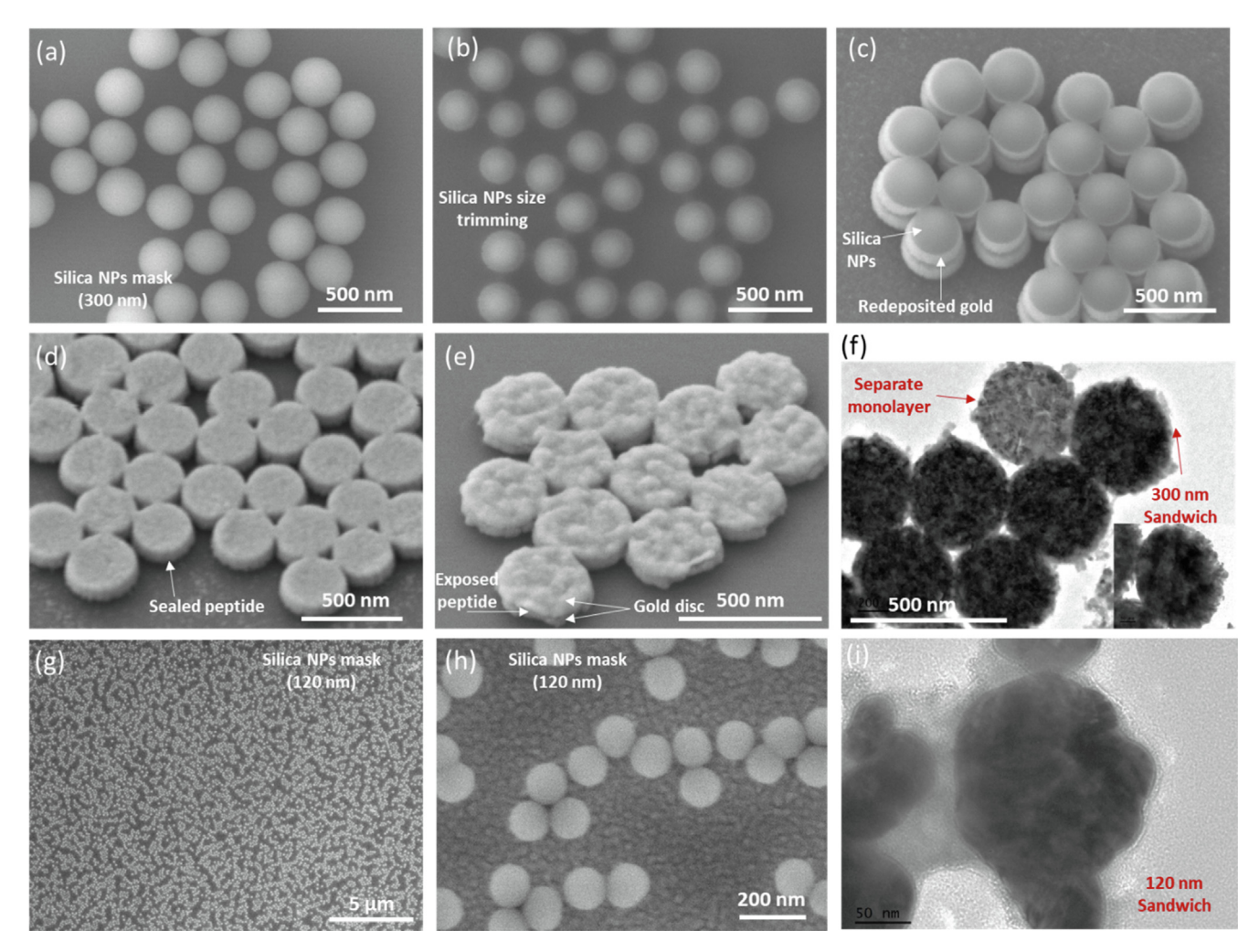


Fig. 3. Morphologies of gold/peptide/gold sandwich NPs during synthesis. (a) Self-assembly of silica NPs (300 nm) on a silicon wafer. (b) Size adjustment of silica NPs mask by CHF₃ etching. (c) Layered nanostructures obtained by directional Ar ion etching. (d) Layered nanostructures after lift-off of the silica NPs masks, where the peptide layer was sealed by redeposited gold during ion etching. (e) Layered gold/peptide/gold nanostructures after removal of redeposited gold through isotropic reactive wet etching. (f) TEM image of the fabricated gold/peptide/gold sandwich NPs (300 nm). (g-h) Self-assembly of silica NPs (120 nm) on a wafer coated with layered gold/polymer/gold structures; (i) TEM image of the fabricated 120 nm gold/polymer/gold sandwich NPs.

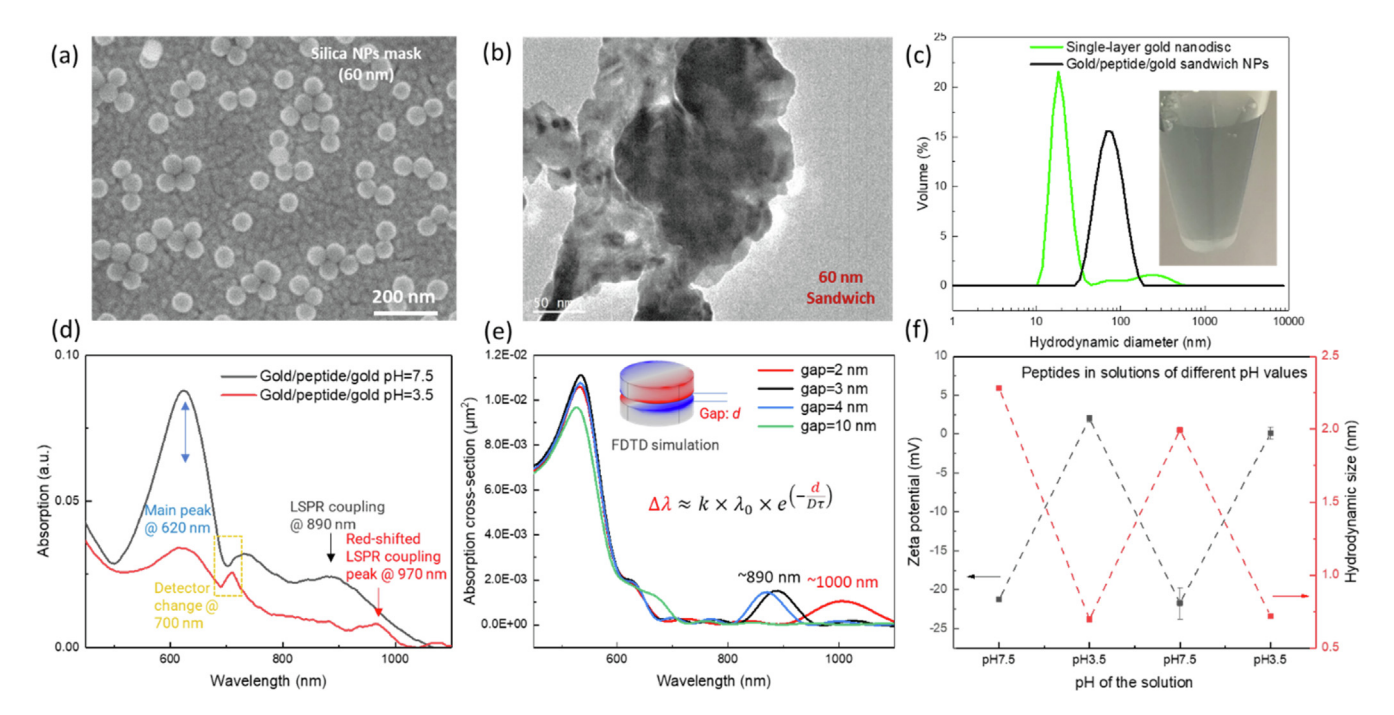


Fig. 4. pH-responsive gold/peptide/gold sandwich NPs with a diameter of 60 nm. (a) Self-assembly of 60 nm silica NPs on a wafer coated with layered gold/polymer/gold structures. (b) TEM image of the fabricated gold/polymer/gold sandwich NPs (60 nm). (c) DLS of gold/peptide/gold sandwich NPs and single-layer gold nanodiscs. The inset shows a digital photograph of gold/peptide/gold sandwich NPs. (d) UV-Vis absorption spectra of gold/peptide/gold sandwich NPs at pH 7.4 and pH 3.5. (e) Simulation results of gap-dependent LSPR coupling absorption peaks in sandwich nanoparticles. (f) Zeta potential and hydrodynamic size of peptides in solutions at different pH values.

3.4. pH-responsive spectral absorption of gold/peptide/gold sandwich nanoparticles

The pH-responsive UV-Vis-NIR absorption spectra of gold/peptide/gold sandwich NPs (60 nm diameter) are shown in Fig. 4d. The gold/peptide/gold sandwich NPs showed the main absorption peak at 620 nm and an LSPR coupling peak in the NIR range. FDTD method was employed to simulate the interparticle gap-induced spectral absorption peak shift of the LSPR coupling, which is well consistent with the measured spectra, as shown in Fig. 4e. The LSPR coupling peaks are related to the plasmonic NPs gap distance [20–22], expressed as:

$$\Delta \lambda \approx k \times \lambda_0 \times e^{(-\frac{d}{D\tau})}$$

where k is the coefficient, d is the separation distance, τ is the decay constant, and D is the diameter of plasmonic NPs. For a structurally defined sandwich nanoparticle, the red shift of the LSPR coupling peak is exponentially correlated to the decrease in distance between Au nanodiscs. At a solution pH of 7.5, the carboxyl group of the peptide in the sandwich nanoparticles was deprotonated and negatively charged, the peptide layer was in a swollen state. This is evidenced by the zeta potential (-25 mV) and hydrodynamic size (2.2 nm) of the freestanding peptide, see Fig. 4f. Therefore, the LSPR coupling peak of the sandwich NPs was located at 890 nm. Although the hydrodynamic size of the freestanding peptide in solution (Fig. 4f) was smaller than the length of the bound peptide within gold/peptide/gold sandwich NPs (Fig. 4d), the change in peptide size in different pH solutions can reflect the change in the length of the peptide in the sandwich NPs. When the solution pH dropped to 3.5, the carboxyl groups of the peptide in the sandwich nanoparticles were protonated and neutralized, and the peptide layer was in a shrinkage state. This is evidenced by the zeta potential of ~ 1 mV and hydrodynamic size of 0.7 nm for the freestanding peptides at pH 3.5. The decrease in the distance between Au nanodiscs under acidic conditions resulted in a red shift of the LSPR coupling peak of the sandwich NPs to 970 nm. Considering the shrinkage and swelling states of the peptide are reversible at different pH, it can be deduced that the LSPR coupling peak shift of the sandwich nanoparticle is also reversible. The pH-adaptive sandwich nanoparticles exhibited an LSPR coupling peak shift of 80 nm, suggesting the potential as pH-adaptive sensors or actuators.

4. Conclusions

A new class of pH-adaptive monodisperse gold/peptide/gold sandwich NPs was synthesized by a liquid-solid phase combined technique. The as-produced gold/peptide/gold nanoparticles show distinct LSPR coupling peaks at NIR wavelength in acidic and neutral environments, showing great potential as pH-responsive optical nanodevices. Furthermore, this flexible and configurable approach enables the preparation of a wide variety of layered nanostructures with designated sizes and compositions for different actuation and sensing applications.

Declaration of Competing Interest

The authors declare that they have no known competing financial interests or personal relationships that could have appeared to influence the work reported in this paper.

Acknowledgments

This work is partially supported by the National Science Foundation (CMMI-1934120, CMMI-1933679) and X-Grant of Texas A&M University.

References

- [1] Chan MS, Landig R, Choi J, Zhou H, Liao X, Lukin MD, et al. Stepwise Ligand-induced Self-assembly for Facile Fabrication of Nanodiamond-Gold Nanoparticle Dimers via Noncovalent Biotin-Streptavidin Interactions. Nano Lett 2019:19:2020-6.
- [2] Sadiq Z, Safiabadi Tali SH, Jahanshahi-Anbuhi S. Gold Tablets: Gold Nanoparticles Encapsulated into Dextran Tablets and Their pH-Responsive

- Behavior as an Easy-to-Use Platform for Multipurpose Applications. ACS Omega 2022;7:11177-89.
- [3] Pastoriza-Santos I, Kinnear C, Pérez-Juste J, Mulvaney P, Liz-Marzán LM. Plasmonic polymer nanocomposites. Nat Rev Mater 2018;3:375–91.
- [4] Li W, Xu F, Liu W, Gao Y, Zhang K, Zhang X, et al. Flexible strain sensor based on aerogel-spun carbon nanotube yarn with a core-sheath structure. Compos A Appl Sci Manuf 2018;108:107–13.
- [5] Deng X, Liang S, Cai X, Huang S, Cheng Z, Shi Y, et al. Yolk-Shell Structured Au Nanostar@ Metal-Organic Framework for Synergistic Chemo-photothermal Therapy in the Second Near-Infrared Window. Nano Lett 2019;19:6772–80.
- [6] Dheyab MA, Aziz AA, Moradi Khaniabadi P, Jameel MS, Oladzadabbasabadi N, Mohammed SA, et al. Monodisperse Gold Nanoparticles: A Review on Synthesis and Their Application in Modern Medicine. Int J Mol Sci 2022;23:7400.
- [7] Lim D-K, Jeon K-S, Hwang J-H, Kim H, Kwon S, Suh YD, et al. Highly uniform and reproducible surface-enhanced Raman scattering from DNA-tailorable nanoparticles with 1-nm interior gap. Nat Nanotechnol 2011;6:452–60.
- [8] Smith BD, Dave N, Huang P-J-J, Liu J. Assembly of DNA-functionalized gold nanoparticles with gaps and overhangs in linker DNA. J Phys Chem C 2011;115:7851-7.
- [9] Song Y, Ding Y, Dong CM. Stimuli-responsive polypeptide nanoassemblies: Recent progress and applications in cancer nanomedicine. Wiley Interdiscip Rev Nanomed Nanobiotechnol 2022;14:e1742.
- [10] Nelson DL, Cox MM, Lehninger AL. Principles of biochemistry. New York: WH Freeman and Company; 2012.
- [11] Esashika K, Ishii R, Tokihiro S, Saiki T. Simple and rapid method for homogeneous dimer formation of gold nanoparticles in a bulk suspension based on van der Waals interactions between alkyl chains. Optical Materials Express 2019;9:1667–77.

- [12] Jiang N, Zhuo X, Wang J. Active plasmonics: principles, structures, and applications. Chem Rev 2017;118:3054–99.
- [13] Dmitriev A, Pakizeh T, Käll M, Sutherland DS. Gold-silica-gold nanosandwiches: tunable bimodal plasmonic resonators. Small 2007;3:294–9.
- [14] Aksu S, Yanik AA, Adato R, Artar A, Huang M, Altug H. High-throughput nanofabrication of infrared plasmonic nanoantenna arrays for vibrational nanospectroscopy. Nano Lett 2010;10:2511–8.
- [15] Juluri BK, Chaturvedi N, Hao Q, Lu M, Velegol D, Jensen L, et al. Scalable manufacturing of plasmonic nanodisk dimers and cusp nanostructures using salting-out quenching method and colloidal lithography. ACS Nano 2011;5:5838-47.
- [16] Li W, Ma J, Garcia S, Gao C, Liu R, Qiu J, et al. Semishell Janus Nanoparticle-Enabled pH-Responsive Rod-Shaped Assembly for Photothermal Therapy. ACS Appl Nano Mater 2021;5:871–80.
- [17] Green T. Gold etching for microfabrication. Gold Bull 2014;47:205–16.
- [18] Sahu AK, Raj S. Effect of plasmonic coupling in different assembly of gold nanorods studied by FDTD. Gold Bull 2022;55:19–29.
- [19] Köhler M. Etching in microsystem technology. John Wiley & Sons; 2008.
- [20] Jain PK, El-Sayed MA. Plasmonic coupling in noble metal nanostructures. Chem Phys Lett 2010;487:153–64.
- [21] Jain PK, Huang WY, El-Sayed MA. On the universal scaling behavior of the distance decay of plasmon coupling in metal nanoparticle pairs: A plasmon ruler equation. Nano Lett 2007;7:2080–8.
- [22] Clarkson JP, Winans J, Fauchet PM. On the scaling behavior of dipole and quadrupole modes in coupled plasmonic nanoparticle pairs. Opt Mater Express 2011;1:970–9.